

**SPLAY-BEND ELASTIC INEQUALITIES SHAPE TACTOIDS, TOROIDS, UMBILICS,
AND CONIC SECTION WALLS IN PARAELECTRIC, TWIST-BEND, AND
FERROELECTRIC NEMATICS***

Oleg D. Lavrentovich,
Advanced Materials and Liquid Crystal Institute,
Materials Science Graduate Program,
Department of Physics,
Kent State University, Kent, OH 4424

Abstract. Elastic constants of splay K_{11} , twist K_{22} , and bend K_{33} of nematic liquid crystals are often assumed to be equal to each other in order to simplify the theoretical description of complex director fields. Here we present examples of how the disparity of K_{11} and K_{33} produces effects that cannot be described in a one-constant approximation. In a lyotropic chromonic liquid crystal, nematic droplets coexisting with the isotropic phase change their shape from a simply-connected tactoid to a topologically distinct toroid as a result of temperature or concentration variation. The transformation is caused by the increase of the splay-to-bend ratio K_{11}/K_{33} . A phase transition from a conventional nematic to a twist-bend nematic implies that the ratio K_{11}/K_{33} changes from very large to very small. As a result, the defects caused by an externally applied electric field change the deformation mode of optic axis from bend to splay. In the paraelectric-ferroelectric nematic transition, one finds an inverse situation: K_{11}/K_{33} changes from small to large, which shapes the domain walls in the spontaneous electric polarization field as conic sections. The polarization field tends to be solenoidal, or divergence-free, a behavior complementary to irrotational curl-free director textures of a smectic A.

This review has been presented as the invited lecture at the 16th European
Conference on Liquid Crystals, July 10-14, 2023, UNICAL-Rende, Italy

INTRODUCTION

Oriental ordering of liquid crystals brings about an important concept of Frank elastic constants K_{ii} describing the energy cost of the gradients in molecular orientations. The Frank constants are of the dimension of a force, and thus can be represented as the ratio of some energy U to a characteristic length l . In a conventional uniaxial nematic (N_U) formed by rod-like molecules, the latter can only be the molecular length, $l \sim 1$ nm. The energy U , as suggested by P.G. de Gennes [1], should be on the order of $k_B T_c$, where k_B is the Boltzmann constant and T_c is the clearing temperature at which the nematic transitions into an isotropic fluid. For $T_c \sim 300$ K, one finds $K_{ii} \sim \frac{U}{l} \sim 4$ pN, which is close to the experimentally measured values. For example, elastic constants of pentylcyanobiphenyl (5CB) are listed [2] at 305 K (about 4 K below the clearing point) as $K_{11} = 4.5$ pN for splay, $K_{22} = 3$ pN for twist, and $K_{33} = 5.5$ pN for bend. In 5CB, as in many other nematics formed by rod-like molecules, the constants follow the trend $K_{33} > K_{11} > K_{22}$ [3, 4, 5, 6]. A relevant geometrical parameter is the aspect length/diameter ratio, which justifies $\frac{K_{11,22}}{K_{33}} < 1$ [3, 4, 5]. K_{22} is somewhat smaller than the other two moduli, which explains why twist often replaces splay and bend in nematic samples deformed by confinement, such as droplets of thermotropic [7, 8, 9, 10, 11] and lyotropic nematics [12, 13]. Although the occurrence of twist in chemically achiral materials [14, 15] is a very interesting topic awaiting its further exploration in the newly discovered ferroelectric nematics [16, 17], this review limits itself to recently described effects caused by a disparity of the splay K_{11} and bend K_{33} moduli. The Frank-Oseen free energy density corresponding to different bulk modes of distortions writes

$$f = \frac{1}{2} K_{11} (\text{div } \hat{\mathbf{n}})^2 + \frac{1}{2} K_{22} (\hat{\mathbf{n}} \cdot \text{curl } \hat{\mathbf{n}})^2 + \frac{1}{2} K_{33} (\hat{\mathbf{n}} \times \text{curl } \hat{\mathbf{n}})^2. \quad (1)$$

The splay and bend geometries are schematized in Fig.1.

There are numerous reasons why K_{11} and K_{33} can be different. If one assumes that the molecules are rigid, then the increase of the length/diameter aspect ratio might decrease K_{11}/K_{33} . However, as noted by R.B. Meyer [18], nematics formed by very long polymer chains should exhibit $K_{11} \gg K_{33}$ since splay creates empty spaces, which must be filled by the ends of molecules to keep the material's density constant. If the molecules are banana-like in shape, a similar inequality, $K_{11} > K_{33}$, is found experimentally [19, 20, 21, 22, 23, 24, 25, 26, 27] and theoretically [4, 28, 29, 30]; see also the recent reviews [31, 32]. An opposite and even stronger disparity of elastic constants is observed in an N_U formed by acute-angle bent core molecules of a shape

resembling a letter λ [33]. The measured splay constant is anomalously weak, $K_{11} = 2$ pN, significantly smaller than the bend constant $K_{33} = 15$ pN and even the twist constant $K_{22} = 5$ pN. The smallness of K_{11} leads to a pronounced bias of defects towards configurations with splay [32, 33].

The low energy cost for bend in banana-like molecules inspired R.B. Meyer [18], I. Dozov [34], R. Memmer [35], and S. M. Shamid et al. [36] to predict the so-called twist-bend nematic (N_{TB}), experimentally found in materials formed by flexible dimeric [29, 37, 38] and rigid bent-core [39] molecules. Another notable result emerging from the smallness of K_{33} is the formation of an oblique helicoidal cholesteric in an external electric [40, 41] or magnetic field [42], predicted by R.B. Meyer [43] and P.G. de Gennes [44].

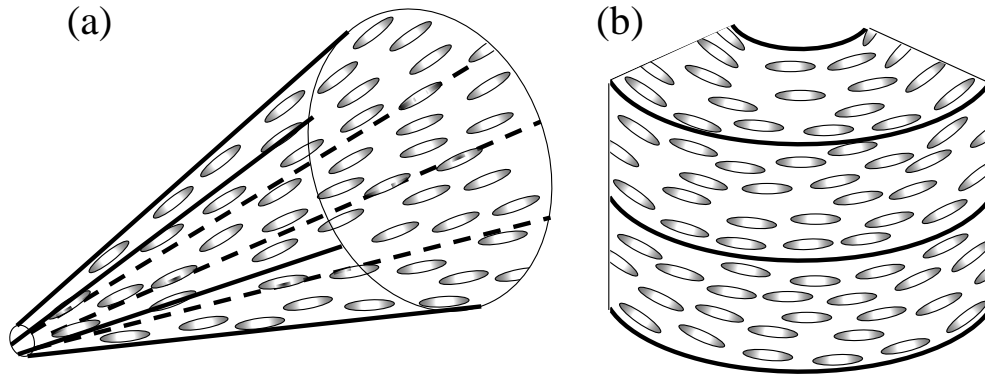


Fig.1. Director field in (a) splay and (b) bend.

In what follows, the presentation discusses (1) topological transformation of a lyotropic chromonic nematic droplet from a tactoid into a toroid driven by the increase of K_{11}/K_{33} changes from large to small, (2) the geometry of defects formed in response to an electric field, which is controlled by a change from $\frac{K_{11}}{K_{33}} \gg 1$ to $\frac{K_{11}}{K_{33}} \ll 1$ as a result of the nematic-to-twist-bend nematic phase transition, and (3) conic sections such as parabola and hyperbola, which represent domain walls in thin films of ferroelectric nematics (N_F) shaped by $\frac{K_{11}}{K_{33}} \gg 1$.

1. Tactoid to toroid reshaping of a nematic droplet: From $K_{11} \approx K_{33}$ to $K_{11} > K_{33}$.

A lyotropic chromonic liquid crystal (LCLC) represents a dispersion of disk-like organic molecules in water. Hydrophobic cores of the molecules stack on top of each other, forming elongated aggregates which align parallel to each other [45]. Elastic constants in the N_U phase depend strongly on the concentration and temperature [2, 46, 47]. One notable experimental finding is that the twist constant K_{22} in the chromonic N_U is anomalously low, less than 1 pN [2, 46, 47]; similar trend is established also for two other lyotropic systems, namely, solutions of the polymer poly- γ -benzyl-glutamate [48] and the N_U formed by disk-like micelles of surfactant molecules [49]. The strong dependence of K_{11} and K_{33} on the temperature and concentration can be interpreted in terms of the varying contour length of the aggregates L and their persistence length λ , i.e., bending flexibility, $K_{11}/K_{33} \propto L/\lambda$ [2, 46]. The increase of K_{11} with L is expected on the grounds of the R.B. Meyer's argument that splay of long molecules is difficult from the entropy point of view, as it creates vacancies that should be filled with the ends of the molecules (or aggregates in the case of LCLCs) [18, 50]. Bend of long rigid rods might create similar problems, but these could be avoided if the molecules (aggregates) are easy to bend, i.e., when λ is small. The anomalous smallness of K_{22} can be qualitatively explained by the fact that twist does not create any "vacancies" if the aggregates arrange in layers perpendicular to the twist axis.

LCLCs exhibit broad biphasic regions in which the N_U (or columnar) phase coexists with the isotropic phase. In coexistence, the aggregates are partitioned between the ordered and disordered phases, with longer aggregates residing in the condensed phase. Prior studies established that the increase of the chromonic concentration c in a homogeneous N_U phase of DSCG increases K_{11}/K_{33} [46]. In the condensed N_U droplets, an increase of the temperature results in a higher concentration of DSCG [51, 52], which in its turn, produces a larger K_{11}/K_{33} responsible for the transformation of the N_U droplets from a sphere-like tactoid to a torus-like toroid [12, 52], Fig.2. These two shapes are topologically distinct, as described by Euler characteristic χ , calculated as $\chi = 2 - 2g$, where g is the number of "handles"; a sphere has no handles, thus $\chi=2$, while a torus is a single handle, thus $\chi=0$.

The biphasic LCLC in Fig.2 represents a water dispersion of disodium cromoglycate (DSCG), of a concentration $c = 0.34$ mol/kg, with an added polyethylene glycol (PEG) as a

condensing agent, at the concentration 0.012 mol/kg. The specimen is made deliberately thin so that the transformation of a thin disk-like tactoid into a torus with a well-defined and wide isotropic central region is clearly visible under a microscope, Fig.2. It starts with the detachment of the two surface point defects-boojuims from the cusps of tactoid, making them two disclinations of strength $+1/2$ each. The disclinations approach each other and coalesce, forming a toroid with a large central isotropic region. A similar transformation is observed when the concentration of PEG increases [52].

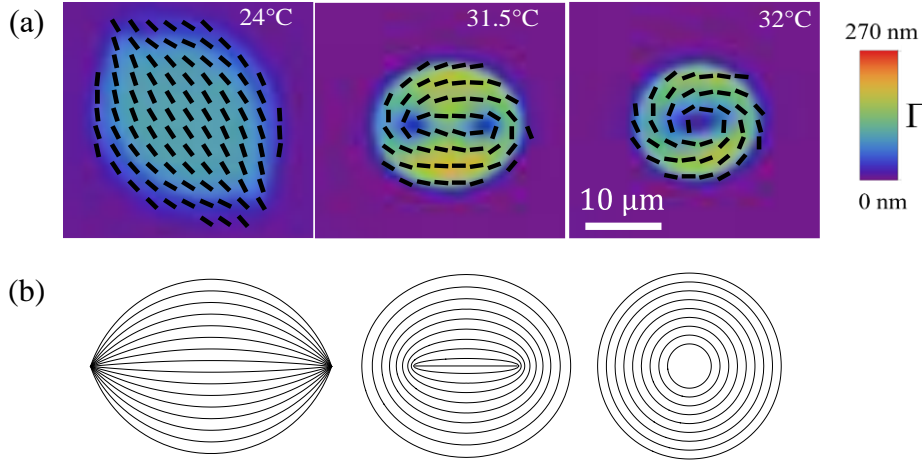


Fig.2. Temperature-triggered tactoid-to-toroid transformation: (a) experimental PolScope textures visualizing the director field; (b) director schemes for analytical estimates. Data from Ref. [52].

As follows from Eq.(1), the elastic energy of a toroid of a radius a and a thickness h with the director written in cylindrical coordinates as $\hat{\mathbf{n}} = \{n_r, n_\psi, n_z\} = \{0, 1, 0\}$, depends only on the elastic constant of bend, $F_{tor} = \pi h K_{33} \ln\left(\frac{a}{r_i}\right)$, where r_i is the radius of the isotropic core. The energy of a circular tactoid of the same volume $hA = \pi h a^2$ and the same surface area A depends also on K_{11} , since splay is present at the cusps, Fig.2b: $F_{tac} \approx \frac{\pi h}{2} K_{11} \ln \frac{2a}{r_{cb}} + \frac{\pi h}{2} K_{33} (1 - \ln 2)$, where r_{cb} is the radius of the core of the boojuims [52]. As K_{11}/K_{33} increases, the first term in the energy F_{tac} increases and the tactoid becomes less energetically favorable as compared to the toroid. The transition condition is $K_{11}/K_{33} > 2$ for $a = 15 \mu\text{m}$, $r_i = r_{cb} = 2 \mu\text{m}$. Surface tension can also contribute to the transformation scenario, but its effect is weaker than that of the elasticity [52]. Numerical simulations, which account for both the elastic and surface energy consideration,

provide a more accurate description of the transition, including the appearance and coalescence of the $\frac{1}{2}$ -disclinations [52].

Out-of-equilibrium and living systems show topological transformations in which χ changes. A cell dividing into two increases the net Euler characteristic from $\chi=2$ to $\chi=4$. An inverse process, a reduction of χ , in which holes are pierced into a sphere, is involved in morphogenesis of multicellular organisms that develop from a spherical cell into torus-like or more complicated multiply-connected bodies [53, 54]. The mechanisms by which living matter employs surface and bulk forces to change topology, especially by decreasing χ , are far from being understood.

Liquid crystal droplets represent a simple model system in which the effect of the bulk and surface forces on the shapes and the internal structure is, in principle, tractable. Droplets of thermotropic liquid crystals dispersed in an immiscible isotropic fluid such as glycerin [55] or in a polymer matrix [56] exhibit a spheroidal shape, $\chi = 2$, imposed by a strong interfacial tension, with a complex interior pattern of molecular orientation that depends on the preferred alignment at the surface. Wei et al. [57] and Peddireddy et al. [58] report on the shape change of N_U droplets from a sphere to branched filamentous networks as a result of a reduction of surface tension. This transformation preserves $\chi=2$. Liquid crystal droplets could also divide at phase transitions, thus increasing χ from 2 to 4, 6, etc., as demonstrated for cholesteric droplets during a transition to a smectic A phase [59]. The tactoid-to-toroid topological transformation [52] adds to this list. When $K_{11} \sim K_{33}$, the droplet accommodates both splay and bend of the director $\hat{\mathbf{n}}$ within a simply-connected tactoid; when K_{11} increases, the droplet could afford only bend, which results in a torus-like shape with a hole in the center, Fig.2.

2. Nematic to twist-bend nematic: From $K_{11} \gg K_{33}$ to $K_{11} \ll K_{33}$.

The twist-bend nematic (N_{TB}) formed by flexible dimers or banana-like molecules exhibits a director field in the shape of a helicoid, maintaining a constant oblique angle $0 < \theta_0 < \pi/2$ with the helix axis $\hat{\chi}$, which we direct along the z axis: $\hat{\mathbf{n}} = \{n_x, n_y, n_z\} = \{\sin \theta_0 \sin \varphi, \sin \theta_0 \cos \varphi, \cos \theta_0\}$, where $\varphi = t_{tb}z$ is the azimuthal angle, $t_{tb} = 2\pi/p_{tb}$, $p_{tb} \sim 10$ nm is the pitch of the helicoid. The reason for this structure is the tendency of molecules to induce a local bend [18, 34, 35, 36]. A pure bend of a constant curvature $|\hat{\mathbf{n}} \times \text{curl} \hat{\mathbf{n}}| = \text{const}$,

however, cannot fill the space. Geometrically, bend $\hat{\mathbf{n}} \times \text{curl}\hat{\mathbf{n}}$ is a vector along the principal normal to the line that envelops the spatially-varying director [60]. The length of this vector at point M is the bend curvature of the line at that point. To maintain a constant bend in space, the line should be of a helicoidal shape. Such a line can be defined on a circular cylinder surface, directed at a constant angle to the axis [31]; this geometry implies twist, which enables a constant bend, hence the name of N_{TB} .

The N_{TB} is typically observed upon cooling of an N_U ; in the latter, the bend tendency manifests itself in a very small K_{33} , which makes K_{11}/K_{33} as high as 30 [25], [31]. Once the N_{TB} emerges upon cooling, the bend could exist only as a nanoscale deformation of the director $\hat{\mathbf{n}}$ but not as a macroscopic deformation of the helicoidal axis $\hat{\chi}$. The reason is that $\hat{\chi}$ is perpendicular to surfaces of a constant azimuthal angle φ : any bend or twist of $\hat{\chi}$ changes the equilibrium p_{tb} , i.e., violates the equidistance of the nanoscale N_{TB} pseudolayers. As a result, the optic axis in the N_U , which is the director $\hat{\mathbf{n}}$, and the optic axis in the N_{TB} , which is $\hat{\chi}$, show dramatically different textures in response to confinement or to an external field, Fig.3.

In the N_U of an N_{TB} -forming mesogen, such as DTC-C9 in Fig.3g, whenever there is a choice between splay and bend, the latter is realized. A good illustration is a Frederiks transition in a sandwich-type cell with homeotropic anchoring. If the material is of a negative dielectric anisotropy, $\Delta\epsilon < 0$, an electric field applied along the normal to the cell causes bend distortions in the vertical plane, which appear as umbilics of a topological charge ± 1 , Fig.3a,e [38]. In the plane of the cell, the director around +1 defects show a clear preference for bend, Fig.3a, which is understandable since $K_{33} \ll K_{11}$. Once the material is cooled down to the N_{TB} phase, the electric field-induced textures of $\hat{\chi}$ are very different, Fig. 3b,c,d,f. Above some threshold voltage, the N_{TB} nucleates circular domains structurally similar to toric focal conic domains in a smectic A, Fig.3c. Further increase of the voltage transforms the circular domains into elongated “oily streaks” which expand and fill the space between the bounding plates [38, 61]. The textures of the optic axis $\hat{\chi}$ show a clear preference to splay, both in the plane of the cell, Fig.3b,c,d, and in the vertical cross-section, Fig.3f. In other words, the N_U -to- N_{TB} transition is accompanied by a change from $\frac{K_{11}}{K_{33}} \gg 1$ for the director $\hat{\mathbf{n}}$ in the N_U to $\frac{K_{11}}{K_{33}} \ll 1$ for the helicoidal axis $\hat{\chi}$ of the N_{TB} .

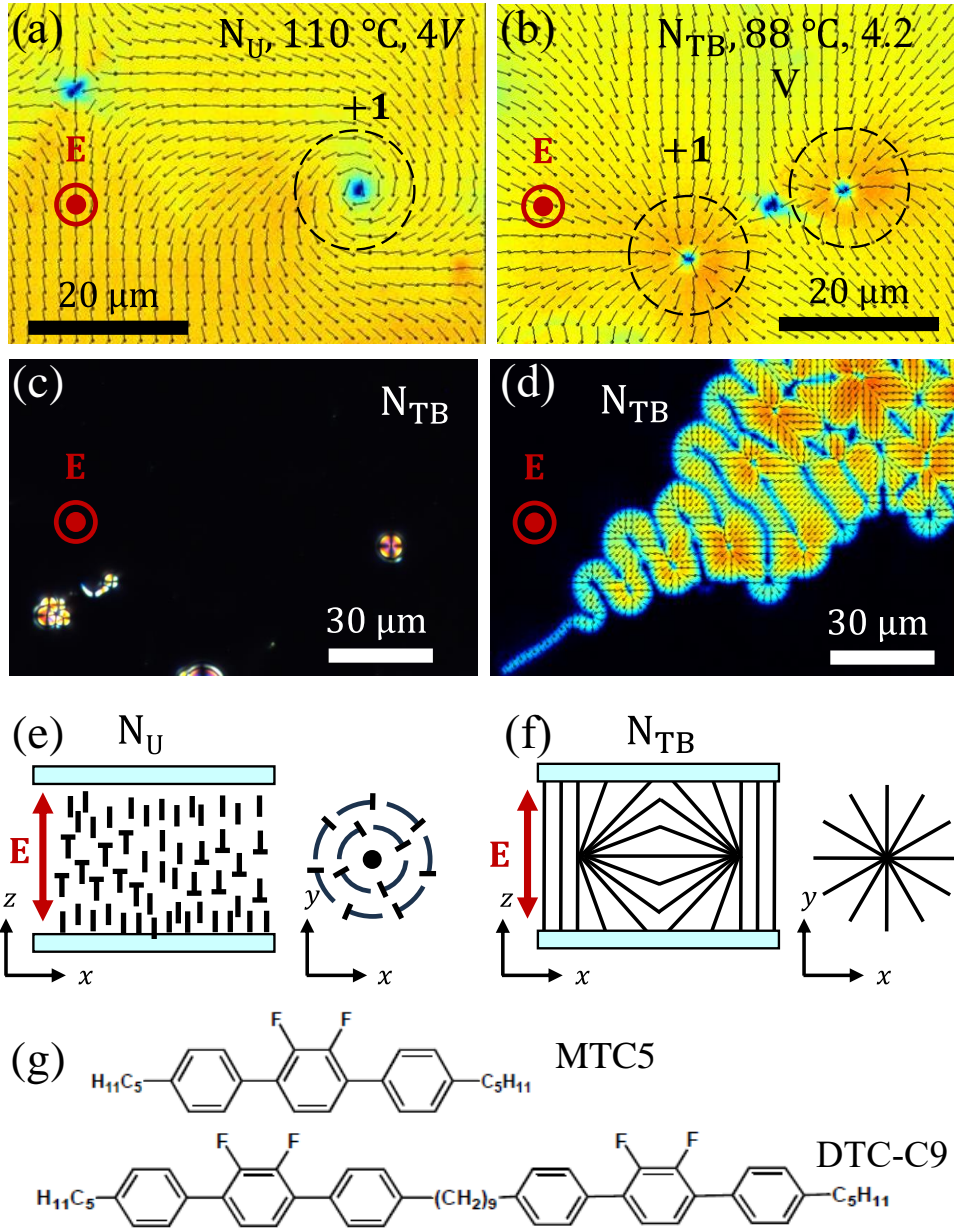


Fig.3. Electric field response of the N_U and N_{TB} with negative dielectric anisotropy in a homeotropic cell: (a) umbilics of the bend Frederiks transition in the N_U caused by the electric field; note the predominance of bend around +1 defect; (b) a field-induced texture of the heliconical axis $\hat{\chi}$ in the N_{TB} ; note the predominance of splay; (c) nucleation and (d) expansion of the realigned N_{TB} structure with splay of $\hat{\chi}$; (e) a scheme of bend in an N_U umbilic; (f) splay of $\hat{\chi}$ in the vertical cross-section of the cell; (g) chemical structure of the N_{TB} -forming composition DTC-C9:MTC5=7:3 by weight. Data from Ref. [38].

3. Nematic to ferroelectric nematic: From $K_{11} \ll K_{33}$ to $K_{11} \gg K_{33}$.

Pioneering exploration [62] of the nematic RM734 formed by molecules with a strong longitudinal dipole moments, ~ 10 D, revealed that the splay constant K_{11} is very small in the N_U phase of this material. The new phase that emerged from the N_U upon cooling, later identified as the uniaxial ferroelectric nematic N_F [63], exhibited textures of domains with oppositely directed spontaneous electric polarization \mathbf{P} in planar cells.

In the N_F , the polarization vector is collinear with the director $\hat{\mathbf{n}}$. Splay is difficult since it produces a bound charge of density $\rho_b = -\text{div } \mathbf{P}$, which increases the electrostatic energy. As envisioned by R.B. Meyer [64] and detailed theoretically in the subsequent studies [65, 66, 67], K_1 associated with $(\text{div } \hat{\mathbf{n}})^2$ is renormalized for the distortions developing over length scales longer than the Debye screening length λ_D : $K_1 = K_{1,0}(1 + \lambda_D^2/\xi_P^2)$, where $K_{1,0}$ is the bare modulus, of the same order as the one normally measured in a conventional paraelectric N_U , $\xi_P = \sqrt{\frac{\epsilon\epsilon_0 K}{P^2}}$ is the so-called polarization penetration length, $\epsilon\epsilon_0$ is the dielectric permittivity of the material, ϵ_0 is the electric constant, $\lambda_D = \sqrt{\frac{\epsilon\epsilon_0 k_B T}{ne^2}}$, e is the elementary electric charge, n is the concentration of ions. For polarization density [68] $P = 5 \times 10^{-2} \text{C/m}^2$ and assumed $\epsilon\epsilon_0 \sim 10^{-9} \frac{\text{C}^2}{\text{J}\cdot\text{m}}$ and $K \sim 10^{-11} \text{N}$, one finds a very short $\xi_P \approx 2$ nm. At the same time, the Debye screening length is expected to be larger: At $T=400$ K, and $n \leq 10^{23}/\text{m}^3$, $\lambda_D \geq 10$ nm. Therefore, the enhancement factor $\frac{\lambda_D^2}{\xi_P^2}$ could be strong and the ratio K_1/K_3 in N_F could be significantly larger than 1.

Very little is known about the elastic constants in the N_U phase of ferroelectric materials and practically nothing is known about the elasticity of N_F . Chen et al [69] measured $K_1 \approx 10K_2$ in the N_U phase of ferroelectric material DIO and expected [67] $K_1 \approx 2$ pN. Mertelj et. al. [62] reported that in the N_U phase of RM734, K_1 is even lower, about 0.4 pN. Since the bend constant K_3 of N_F is not expected to experience electrostatic renormalization, it could be a few tens of pN; Mertelj et. al. [62] found $K_3 \approx 10\text{-}20$ pN for the N_U phase of RM734.

The role of space charge in shaping elastic anisotropy of bend vs splay has been extensively studied in the past for the ferroelectric chiral smectic C* (SmC*) [66, 70, 71, 72, 73]. Since the polarization vector in SmC* is perpendicular to the long axes of molecules, electrostatic effects lead to a large K_3 , as discussed by Link et al. [71] and Pattanaporkratana et al. [72] for -1 disclinations, Zhuang [70] and Dolganov et al. [74] for 2π domain walls. In the N_F , electrostatic effects increase K_1 rather than K_3 since \mathbf{P} is parallel to the long molecular axes; besides, these effects might be stronger than in the SmC* since the polarization of the N_F is higher.

A qualitative evidence that $K_1 > K_3$ in the N_F is presented by the textures of planar monocrystalline N_F samples with air bubbles trapped between glass plates [75], Fig.4, domain walls in planar cells with rubbed substrates [76] and walls in thin azimuthally degenerate films in which the spatial variations of the polarization are not restricted by the externally imposed rubbing directions, Fig.5 [77].

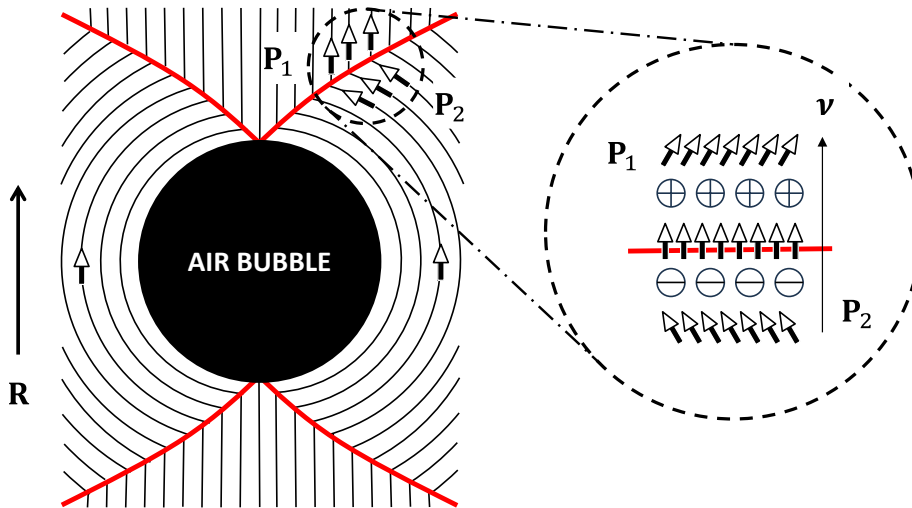


Fig.4. Parabolic domain walls caused by an air bubble in a planar N_F cell. The parabola bisects the two polarization fields, a uniform \mathbf{P}_1 and a circular \mathbf{P}_2 . The inset shows how the in-plane realignment of \mathbf{P} leads to two sheets of opposite charges which attract each other thus stabilizing the wall. \mathbf{R} is the rubbing direction on both plates of the sandwich-type sample; \mathbf{v} is an axis perpendicular to the wall. Redrawn from [75].

In a planar cell with a trapped air bubble, Fig.4, the polarization vector is subject to a frustration between the unidirectional rubbing of the substrates which aligns \mathbf{P} uniformly along the rubbing direction \mathbf{R} , and the circular interface of the bubble, which aligns \mathbf{P} tangentially to

itself. The frustration is resolved by four parabolic branches, emerging from the poles of the droplet and separating the domain of a circular \mathbf{P}_2 around the air bubble and the uniform far-field \mathbf{P}_1 dictated by the rubbing, Fig.4. This structure avoids splay thus the space charge is minimum, and the parabolic domain walls avoid being charged since they bisect the uniform and circular polarization fields [75]. In the description of the domain wall defect, one often assumes that the polarization vector remains in the plane of the wall [70, 72, 75], i.e., in the plane of Fig.4. If that is the case, then the projection $\mathbf{P} \cdot \mathbf{v} = P_v$ of the polarization vector onto the axis \mathbf{v} normal to the wall increases while transitioning from \mathbf{P}_1 to \mathbf{P}_2 . As a result, the derivative $-\partial P_v / \partial v$, which is the space charge density, produces two oppositely charged sheets attracting each other [70, 72, 75]. Electrostatic attraction is opposed by orientational elasticity [70, 72, 75]. The balance of the two yields an estimate of the domain wall width as the polarization penetration length [70], $\xi_P = \sqrt{\frac{\epsilon \epsilon_0 K}{P^2}} \sim 1$ nm, which is very short [70, 72, 75].

It turns out that parabolic as well as hyperbolic domain walls could form in the absence of externally imposed unidirectional rubbing and the entrapped air bubbles, as an intrinsic feature of the distorted polarization fields $\mathbf{P}(\mathbf{r})$ in samples in which the boundary conditions impose no restriction on the in-plane alignment of \mathbf{P} , Fig.5 [76, 77]. The polarization field tends to form vortices to reduce the effects of depolarization field. Consider two situations. In one, the N_F polarization within a sample of an area $A = L^2$ and thickness h , is uniform, $\mathbf{P} = \{P_x, P_y, P_z\} = P\{1, 0, 0\}$. It means that the two yz sides of the sample are charged with the surface densities $\pm P$. The corresponding depolarization field and the electrostatic energy are then $\mathbf{E}_{DP} = -\frac{\mathbf{P}}{\epsilon \epsilon_0}$ and $U_{DP} = \frac{P^2 L^2 h}{\epsilon \epsilon_0}$, respectively. There is no elastic energy as the polarization is uniform. Consider now a circular disk sample of the same area $A = L^2$ and thickness, in which \mathbf{P} forms a circular vortex; in cylindrical coordinates, $\mathbf{P} = \{P_r, P_\psi, P_z\} = P\{0, 1, 0\}$. Since \mathbf{P} is everywhere tangential to the surface and since there is no splay, the only energy is that one of the elastic bend [60]: $U_{bend} = \pi K_{33} h \ln \frac{L}{r_{core}} + U_{core}$, where r_{core} and $U_{core} \sim \pi K_{33} h$ are the molecular scale radius and the energy of the vortex' core, respectively; U_{core} brings an inessential contribution to U_E and can be absorbed into the rescaled r_{core} . The ratio of the energies of the two structures is then $\frac{U_{DP}}{U_{bend}} = \frac{P^2 L^2}{\pi \epsilon \epsilon_0 K_{33} \ln \frac{L}{r_{core}}}$

. With $L = 10 \text{ } \mu\text{m}$, $\ln \frac{L}{r_{core}} \sim 10$, and the estimates above, $\frac{U_{DP}}{U_{bend}} \sim 10^6$, a huge number. It is only when $L \sim 10 \text{ nm}$, close to ξ_P , that the two states show a similar energy. Of course, the surface polarization charges can be screened by charges of free ions, so that the depolarization field is reduced to $E_{DP} = -\frac{P+\sigma_s}{\epsilon\epsilon_0}$. The typical surface charge of adsorbed ions reported for nematics [78, 79] is rather weak, $\sigma_s \sim (10^{-4} - 10^{-5}) \text{ C m}^{-2}$, smaller than $P \approx (4 - 6) \times 10^{-2} \text{ C m}^{-2}$. Although higher values of σ_s are possible, see the discussion below, one might still expect that vortex states of N_F films with azimuthally degenerate anchoring are energetically similar or even preferable than extended areas of a uniform polarization.

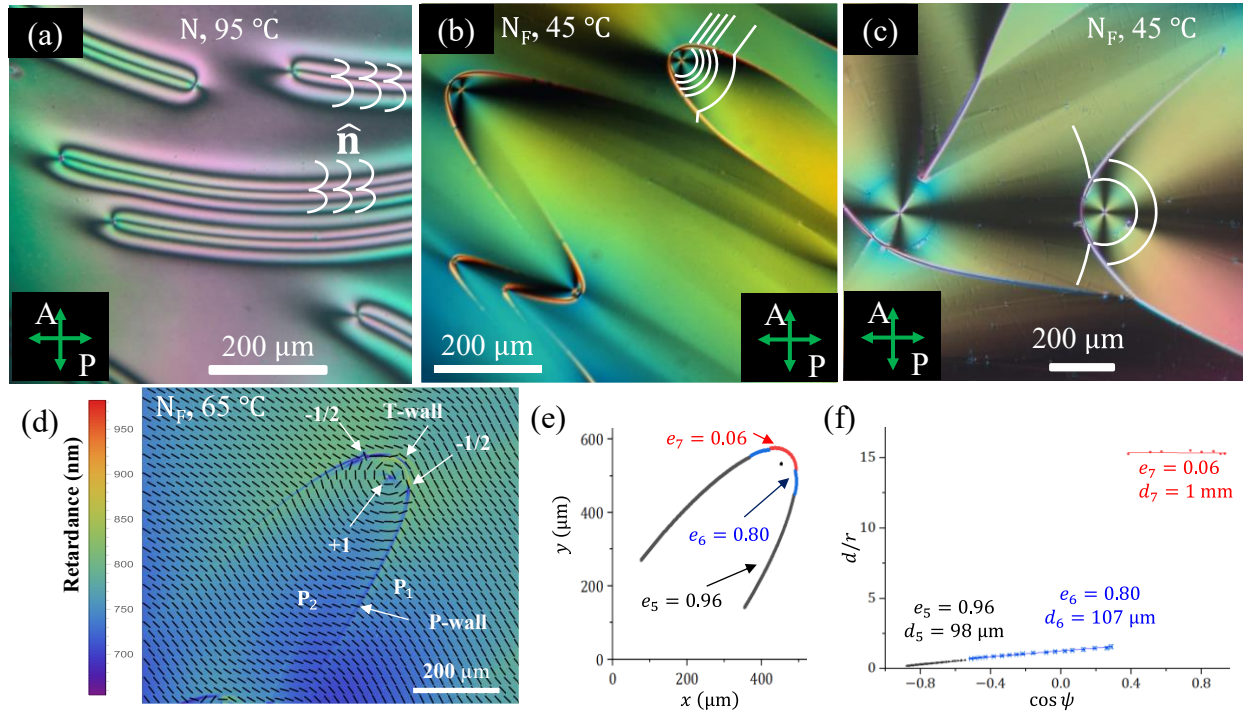


Figure 5. DIO N_F thin films at a glycerin substrate. (a) N_U film with 2π splay-bend domain walls; (b,c), N_F texture of conic-sections with prevailing circular bend and parabolic (b) or (c) hyperbolic domain walls; \hat{n} is depicted by white lines in (a-c); (d) parabolic domain wall separating a +1 vortex from a relatively uniform domain; note a composite defect representing a T-wall limited by two -1/2 disclinations, visualized by PolScope; (e) eccentricity of different parts of the parabolic wall in (d); (f) fitting the conic in (d) with directrix and eccentricity. Data from Ref.[77].

The samples are prepared by spreading a thin (few micrometers) film of N_F onto the surface of immiscible fluid, such as glycerin. Alternatively, one can use coatings with polymers such as polystyrene that impose no in-plane azimuthal preference for the orientation of N_U [80] and N_F [77]. Since the N_F exhibits no crystallographic axes, these N_F samples set no preferred direction of \mathbf{P} , except that \mathbf{P} tends to be tangential to the interface to avoid depositing charges on it.

Figure 5a-c shows the textures of thin DIO films spread onto the surface of glycerin; the upper surface is free. In the N_U phase, hybrid alignment of the director, tangential at the glycerin and homeotropic at the free surface, leads to 2π domain walls of the “W” director geometry [81]; these 2π domain walls contain both splay and bend and are clearly distinguished in Fig.5a as bands with four extinction bands. In the N_F , the director and \mathbf{P} are tangential to both the N_F -glycerin and N_F -air interfaces. The most important feature is that the curvature lines of \mathbf{P} and $\hat{\mathbf{n}}$ in the N_F are close to circles and circular arches, which implies prevalence of bend and formation of +1 vortices $\mathbf{P} = \{P_r, P_\psi, P_z\} = P\{0,1,0\}$, Fig.5b,c. Each vortex is separated from a uniform or nearly uniform \mathbf{P} by walls shaped as parts of ellipses and parabolas, Figs. 5b, while two neighboring +1 vortices are separated by hyperbolic walls, Fig. 5c.

The shapes of domain walls are verified with an equation of a conic, written in polar coordinates (r, ψ) centered at the core of a circular vortex, as

$$\frac{d}{r} = \frac{1}{e} - \cos \psi, \quad (2)$$

where e is the eccentricity, d is the distance from the core to the directrix. The domain walls satisfy Eq.(1) with either $e \approx 1$ (parabolic, or P-walls) or $e > 1$ (hyperbolic, or H-walls) everywhere, except for the tip regions. Near the tips, the fits yield a much smaller e characteristic of elliptical and circular arcs; these arcs are abbreviated as T-walls. The T-walls are 180° DWs, separating two antiparallel polarizations, \mathbf{P} and $-\mathbf{P}$, and limited by two $-1/2$ disclinations.

The shapes of P- and H-walls are dictated by the N_F tendency to form vortex states and avoid bound electric charge [77]. The equivalent of the bulk bound electric charge is the interfacial charge of density $\sigma_b = (\mathbf{P}_1 - \mathbf{P}_2) \cdot \hat{\mathbf{v}}_1$, where $\hat{\mathbf{v}}_1$ is the unit normal to a domain wall, pointing from domain 2 towards domain 1. Away from the domain walls and the cores of circular vortices, $|\mathbf{P}_1| = |\mathbf{P}_2| = P$. To be uncharged, a domain wall must bisect the angle between \mathbf{P}_1 and \mathbf{P}_2 , so that $\mathbf{P}_1 \cdot$

$\hat{\mathbf{v}}_1 = \mathbf{P}_2 \cdot \hat{\mathbf{v}}_1$, which means that the components of the polarization along the normal to the wall are continuous and equal each other while the projections onto the wall are antiparallel.

The remarkable bisecting properties of conics, elucidated millennia ago by Apollonius of Perga [82], are often formulated in terms of light reflection [83]. Consider a parabola, Fig.6a. Light emitted from a focus, which is the core of the circular vortex in the N_F case, is reflected by the parabola along the lines parallel to the symmetry axis. A tangent to a parabola at a point (x, y) makes equal angles with the radius-vector directed from the focus and with the reflected beam. Equivalently, the angle θ_1 between \mathbf{P}_1 and the P-wall and the angle θ_2 between \mathbf{P}_2 and the P-wall are equal, Fig.6a,

$$\theta_1 = \theta_2 = \arctan \sqrt{\frac{x}{f}}, \quad (3)$$

where $\eta =$ and the origin of the Cartesian coordinates (x, y) is at the conic's vertex. Therefore, when a P-wall separates a circular vortex of \mathbf{P}_2 from a uniform domain with \mathbf{P}_1 orthogonal to the parabola's axis, its parabolic shape guarantees that $\mathbf{P}_1 \cdot \hat{\mathbf{v}}_1 = \mathbf{P}_2 \cdot \hat{\mathbf{v}}_1$ and carries no surface charge, $\sigma_b = 0$. The bulk charge ρ_b is also zero since there is no splay of \mathbf{P}_1 and \mathbf{P}_2 . The H-wall features a similar bisecting property which assures a zero σ_b at the boundary between two vortices, Fig.6b.

One expects that the variation of the projection of \mathbf{P} onto $\hat{\mathbf{v}}_1$ across the wall would create two sheets of opposite charges if \mathbf{P} remains in the plane of the sample [70, 72, 75], as in a Néel wall in ferroelectric crystals; these two charged sheets are shown in Fig.4. Note that in the textures in Fig.5, the width w of the P- and H- walls is $\sim 10 \mu\text{m}$ [77], much wider than $\xi_P \sim \sqrt{\frac{\varepsilon \varepsilon_0 K}{P^2}} \sim 1 \text{ nm}$. One reason is that the polarization is screened by ions, so that the domain width can be estimated as $w \sim \sqrt{\frac{\varepsilon \varepsilon_0 K}{(P + \sigma)^2}}$. With $\varepsilon \varepsilon_0 \sim 10^{-9} \frac{\text{C}^2}{\text{J} \times \text{m}}$, $K \sim 10^{-11} \text{ N}$, $w \sim 10 \mu\text{m}$, one finds $P + \sigma \approx 10^{-5} \frac{\text{C}}{\text{m}^2}$, a three orders of magnitude reduction from the un-screen polarization. One should not exclude also the possibility of the twist of \mathbf{P} , either around an in-plane axis, as in a Bloch wall, or around the twist axis which is perpendicular to the film.

The combined defects representing a T-wall sandwiched between two $-1/2$ disclinations are caused by the fact that the bend angle δ between the vectors \mathbf{P}_1 and \mathbf{P}_2 near the vertex

increases, making the polarization field “hairpin”-like, Fig.6c. The $-1/2$ disclinations replace this large bent angle $\delta = \pi - 2\theta$ with two small angles $\beta \approx \theta$, thus reducing the bend energy [77].

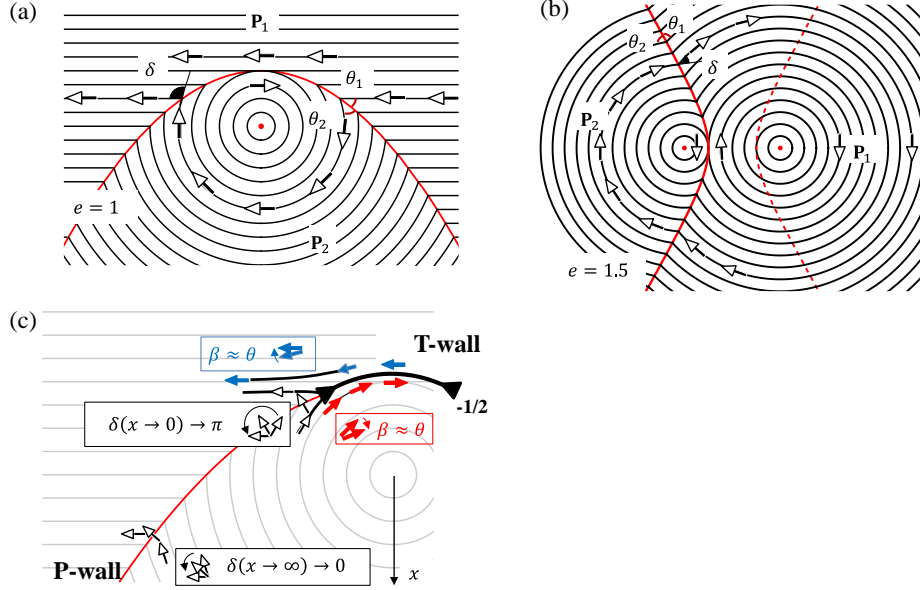


Fig.6. Schemes of (a) parabolic, (b) hyperbolic, and (c) T-walls sandwiched between two $-1/2$ disclinations. Data from Ref.[77].

The composite defects representing T-walls bounded by half-integer disclinations have been predicted for N_F [84, 85] as analogs of the domain walls seeded by cosmic strings in the early Universe models [86] and of domain walls bounded by half-quantum vortices recently found in a superfluid ^3He [87, 88]. In the Universe and ^3He scenarios, the composite domain walls appear after a phase transition from a symmetric phase that contains isolated strings/disclinations. In the less symmetric phase, the isolated disclinations are topologically prohibited and must be connected by a domain wall. In contrast, the $-1/2$ disclinations at the ends of T-walls described by Kumari et al. [77] serve to reduce the elastic energy of strong bends, Fig.6c, and appear without any reference to the potential seeds in the more symmetric phase.

In 1910, G. Friedel and F. Grandjean [89] described ellipses and hyperbolas seen under a microscope in a liquid crystal of a type unknown at that time. A later analysis [90, 91] revealed that these conics are caused by a layered structure of the liquid crystal known nowadays as a smectic A (SmA). The layers are flexible but preserve equidistance when curled in space. The

director $\hat{\mathbf{n}}$ is normal to the equidistant layers and can experience only splay but not twist nor bend. The families of flexible equidistant surfaces form focal surfaces at which the layers curvatures diverge. To reduce the energy of these singular focal surfaces, the SmA reduces them to lines of confocal conics, such as an ellipse-hyperbola or two parabolas [92]; these pairs form the frame of the celebrated focal conic domains (FCDs) [60]. Gray lines in Fig. 6 could be interpreted as cuts of smectic layers wrapped around a parabola and hyperbola of FCDs, Fig.7. The N_F conics are shaped by a different mechanism, rooted in the avoidance of the space charge. In the N_F , $\hat{\mathbf{n}}(\mathbf{r})$ and $\mathbf{P}(\mathbf{r})$ tend to be solenoidal, $\text{div}\hat{\mathbf{n}} = \text{div}\mathbf{P} = 0$, while the director in SmA is irrotational, $\text{curl}\hat{\mathbf{n}} = 0$. Besides this difference in physical underpinnings, there is also a distinction in how the conics in the N_F and SmA heal cusp-like singularities. In the N_F , the cusps are attended by a bend of the polar vector \mathbf{P} , which necessitates the $-1/2$ disclinations and the T-walls at the tips of the conics, while in the SmA, a similar cusp could be healed by weak splay of the apolar director $\hat{\mathbf{n}} \equiv -\hat{\mathbf{n}}$.

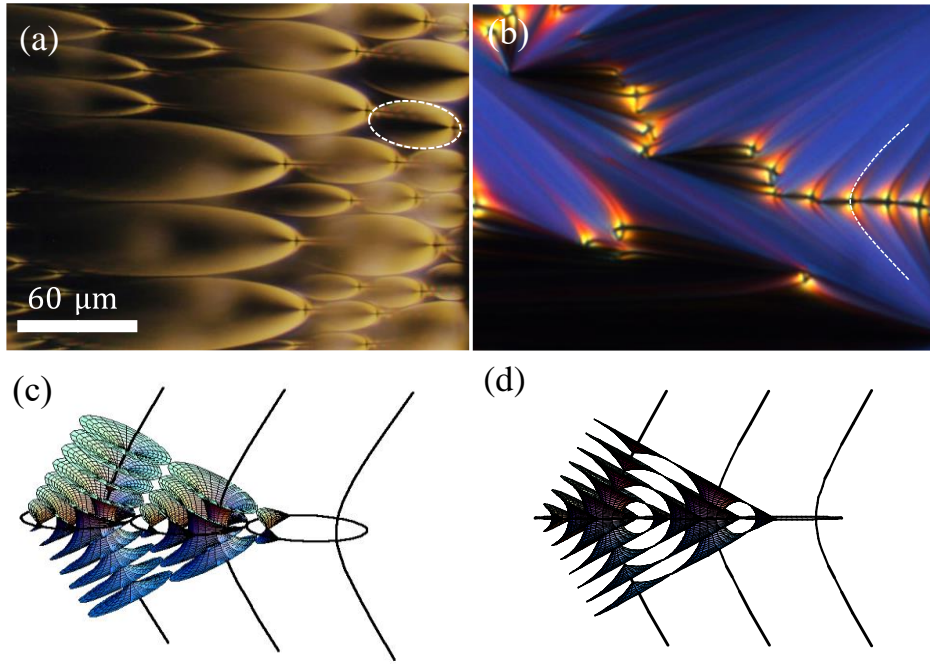


Fig. 7. Smectic A textures of focal conic domains with (a) ellipses in the plane of the sample; (b) hyperbolas in the plane of the sample; (c,d) two 3D views of SmA domain walls formed by focal conic domains.

CONCLUSION

As indicated by de Gennes [1], the full form of the Frank-Oseen energy (1) is “too complex to be of practical use,” either because the values of the corresponding elastic constants are not known or because the equations are prohibitively difficult to solve. One often resorts to the so-called one-constant approximation in which all constants are assumed to be equal. The presented examples underscore the importance of elastic constants disparity. The problems might still be “simple” when only a few types of distortions are at play, such as splay and saddle-splay in the description of FCDs in SmA [93]. So far, the textures of the N_F have been explored for relatively thin quasi-2D films. Bulk samples with a 3D divergence-free polarization field might reveal more complex structures. For example, I. Luk’yanchuk et al. [94] predicted that a small spherical particle of solid ferroelectrics should produce a hopfion, which is a set of interlinked circles. Hopfions have been already observed in liquid crystals such as nematic-based ferromagnets by I.I. Smalyukh et al. [95, 96, 97]. A need for a hopfion in 3D can be justified by the argument that \mathbf{P} is everywhere tangential to the spherical surface but instead of forming a singular vortex-like disclination, it features a core with \mathbf{P} escaped into the third dimension [94], a notion well known in the physics of disclinations in liquid crystals [98, 99]. Droplets of N_F might be a natural home for hopfions.

The list of new discoveries has been recently extended by the twist-bend ferroelectric nematic N_{TBF} , synthesized at the Military University of Technology in Poland [100]. The new phase, formed by achiral polar molecules, with a spontaneous electric polarization along the heliconical axis, is a ferroelectric analog of the paraelectric N_{TB} . The pseudolayers of the N_{TBF} , associated with the constant phase of the molecular tilts, tend to keep equidistance, which hinders the twist and bend of the heliconical axis. On the other hand, splay of this axis is also hindered, since it creates space charge. Remarkably, the pitch of heliconical N_{TBF} structure is in the submicron range and changes under an externally applied dc electric field. At higher field, the structure shows a shorter pitch and a smaller conical angle, eventually unwinding into a uniform nematic structure, a behavior analogous to the paraelectric response of the oblique helicoidal cholesteric [40, 41, 101].

The author is thankful to N. A. Clark, D. Golovaty, A. Jákli, M.O. Lavrentovich, I. Luk’yanchuk, Yu. A. Nastishin, S. Paul, S.V. Shiyonovskii, P.J. Sternberg, H.Wang, for useful discussions, to the graduate students A. Alqarni, G. Babakhanova, B. Basnet, V. Borshch, Y.-K.

Kim, R. Koizumi, P. Kumari, B-X. Li, M. Rajabi, J. Xiang, who performed most of the experiments reviewed in this paper, and to the organizers of the 16th European conference on liquid crystals at the University of Calabria in Rende, Italy, for the opportunity to present these results.

Disclosure statement

No potential conflict of interest was reported by the author.

Funding

The work is supported by the NSF grants DMS-2106675, DMR-2122399, and DMR-2215191.

ORCID

Oleg D. Lavrentovich <http://orcid.org/0000-0002-0128-0708>

Author contributions

O.D.L. wrote the paper.

Data availability statement

The data that support the findings of this study are available within the manuscript.

REFERENCES

1. de Gennes PG, Prost J. The Physics of Liquid Crystals. Oxford: Clarendon Press; 1993.
2. Zhou S, Neupane K, Nastishin YA, Baldwin AR, Shiyanovskii SV, Lavrentovich OD, Sprunt S. Elasticity, viscosity, and orientational fluctuations of a lyotropic chromonic nematic liquid crystal disodium cromoglycate. *Soft Matter*. 2014;10:6571-81.
3. Odijk T. Elastic-Constants of Nematic Solutions of Rod-Like and Semiflexible Polymers. *Liq Cryst*. 1986;1:553-9.
4. Revignas D, Ferrarini A. Microscopic modelling of nematic elastic constants beyond Straley theory. *Soft Matter*. 2022;18:648-61.
5. Singh S. Curvature elasticity in liquid crystals. *Phys Rep*. 1996;277:284-384.
6. De Jeu WH, Claassen WAP. Elastic-Constants of Nematic Liquid-Crystalline Terminally Substituted Azoxybenzenes. *J Chem Phys*. 1977;67:3705-12.
7. Volovik GE, Lavrentovich OD. Topological Dynamics of Defects: Boojums in Nematic Drops. *Sov Phys JETP*. 1983;58:1159-66.
8. Williams RD. Two Transitions in Tangentially Anchored Nematic Droplets. *J Phys a-Math Gen*. 1986;19:3211-22.
9. Lavrentovich OD, Sergan VV. Parity-Breaking Phase-Transition in Tangentially Anchored Nematic Drops. *Nuovo Cimento D*. 1990;12:1219-22.
10. Lavrentovich OD, Terent'ev EM. Phase transition altering the symmetry of topological point defects (hedgehogs) in a nematic liquid crystal. *Sov Phys JETP*. 1986;1986:1237-44.
11. Drzaic PS. A case of mistaken identity: spontaneous formation of twisted bipolar droplets from achiral nematic materials. *Liq Cryst*. 1999;26:623-7.
12. Tortora L, Lavrentovich OD. Chiral symmetry breaking by spatial confinement in tactoidal droplets of lyotropic chromonic liquid crystals. *Proceedings of the National Academy of Sciences of the United States of America*. 2011;108:5163-8.
13. Jeong J, Davidson ZS, Collings PJ, Lubensky TC, Yodh AG. Chiral symmetry breaking and surface faceting in chromonic liquid crystal droplets with giant elastic anisotropy. *Proceedings of the National Academy of Sciences of the United States of America*. 2014;111:1742-7.
14. Hough LE, Spannuth M, Nakata M, Coleman DA, Jones CD, Dantlgraber G, Tschierske C, Watanabe J, Korblova E, Walba DM, MacLennan JE, Glaser MA, Clark NA. Chiral Isotropic Liquids from Achiral Molecules. *Science*. 2009;325:452-6.
15. Hough LE, Jung HT, Kruerke D, Heberling MS, Nakata M, Jones CD, Chen D, Link DR, Zasadzinski J, Heppke G, Rabe JP, Stocker W, Korblova E, Walba DM, Glaser MA, Clark NA. Helical Nanofilament Phases. *Science*. 2009;325:456-60.
16. Khachatryan AG. Development of Helical Cholesteric Structure in a Nematic Liquid-Crystal Due to Dipole-Dipole Interaction. *J Phys Chem Solids*. 1975;36:1055-61.
17. Kumari P, Basnet B, Lavrentovich MO, Lavrentovich OD. Chiral ground states of ferroelectric liquid crystals. *ArXiv*. 2024:2401.09675.
18. Meyer RB. Structural Problems in Liquid Crystal Physics. In: Balian R, Weill G, editors. *Molecular Fluids Les Houches Lectures*, 1973. Les Houches Gordon and Breach; 1976. p. 271-343.
19. Dilisi GA, Terentjev EM, Griffin AC, Rosenblatt C. Viscoelastic Properties of a Bent and Straight Dimeric Liquid-Crystal. *J Phys Li*. 1993;3:597-602.
20. Sathyanarayana P, Mathew M, Li Q, Sastry VSS, Kundu B, Le KV, Takezoe H, Dhara S. Splay bend elasticity of a bent-core nematic liquid crystal. *Phys Rev E*. 2010;81:010702(R).
21. Majumdar M, Salamon P, Jáklí A, Gleeson JT, Sprunt S. Elastic constants and orientational viscosities of a bent-core nematic liquid crystal. *Phys Rev E*. 2011;83:031701.

22. Adlem K, Čopič M, Luckhurst GR, Mertelj A, Parri O, Richardson RM, Snow BD, Timimi BA, Tuffin RP, Wilkes D. Chemically induced twist-bend nematic liquid crystals, liquid crystal dimers, and negative elastic constants. *Physical review E, Statistical, nonlinear, and soft matter physics*. 2013;88:022503.
23. Avci N, Borshch V, Sarkar DD, Deb R, Venkatesh G, Turiv T, Shiyankovskii SV, Rao NVS, Lavrentovich OD. Viscoelasticity, dielectric anisotropy, and birefringence in the nematic phase of three four-ring bent-core liquid crystals with an L-shaped molecular frame. *Soft Matter*. 2013;9:1066-75.
24. Kaur S, Liu H, Addis J, Greco C, Ferrarini A, Gortz V, Goodby JW, Gleeson HF. The influence of structure on the elastic, optical and dielectric properties of nematic phases formed from bent-core molecules. *J Mater Chem C*. 2013;1:6667-76.
25. Cukrov G, Golestani YM, Xiang J, Nastishin YA, Ahmed Z, Welch C, Mehl GH, Lavrentovich OD. Comparative analysis of anisotropic material properties of uniaxial nematics formed by flexible dimers and rod-like monomers. *Liq Cryst*. 2017;44:219-31.
26. Babakhanova G, Parsouzi Z, Paladugu S, Wang H, Nastishin YA, Shiyankovskii SV, Sprunt S, Lavrentovich OD. Elastic and viscous properties of the nematic dimer CB7CB. *Phys Rev E*. 2017;96:062704.
27. Babakhanova G, Wang H, Rajabi M, Li D, Li Q, Lavrentovich OD. Elastic and electro-optical properties of flexible fluorinated dimers with negative dielectric anisotropy. *Liq Cryst*. 2022;49:982-94.
28. Cestari M, Frezza E, Ferrarini A, Luckhurst GR. Crucial role of molecular curvature for the bend elastic and flexoelectric properties of liquid crystals: mesogenic dimers as a case study. *J Mater Chem*. 2011;21:12303-8.
29. Cestari M, Diez-Berart S, Dunmur DA, Ferrarini A, de la Fuente MR, Jackson DJ, Lopez DO, Luckhurst GR, Perez-Jubindo MA, Richardson RM, Salud J, Timimi BA, Zimmermann H. Phase behavior and properties of the liquid-crystal dimer 1'',7''-bis(4-cyanobiphenyl-4'-yl) heptane: a twist-bend nematic liquid crystal. *Physical review E, Statistical, nonlinear, and soft matter physics*. 2011;84:031704.
30. Revignas D, Ferrarini A. Interplay of Particle Morphology and Director Distortions in Nematic Fluids. *Phys Rev Lett*. 2020;125:267802.
31. Jákli A, Lavrentovich OD, Selinger JV. Physics of liquid crystals of bent-shaped molecules. *Rev Mod Phys*. 2018;90:045004.
32. Jákli A, Nastishin Y, Lavrentovich OD. Defects in bent-core liquid crystals. *Liquid Crystals Reviews*. 2023;11:10.1080/21680396.2022.2086932.
33. Li BX, Nastishin YA, Wang H, Gao M, Paladugu S, Li R, Fukuto M, Li Q, Shiyankovskii SV, Lavrentovich OD. Liquid crystal phases with unusual structures and physical properties formed by acute-angle bent core molecules. *Physical Review Research*. 2020;2:033371.
34. Dozov I. On the spontaneous symmetry breaking in the mesophases of achiral banana-shaped molecules. *Europhys Lett*. 2001;56:247-53.
35. Memmer R. Liquid crystal phases of achiral banana-shaped molecules: a computer simulation study. *Liq Cryst*. 2002;29:483-96.
36. Shamid SM, Dhakal S, Selinger JV. Statistical mechanics of bend flexoelectricity and the twist-bend phase in bent-core liquid crystals. *Phys Rev E*. 2013;87:052503.
37. Chen D, Porada JH, Hooper JB, Klittnick A, Shen YQ, Tuchband MR, Korblova E, Bedrov D, Walba DM, Glaser MA, MacLennan JE, Clark NA. Chiral heliconical ground state of nanoscale pitch in a nematic liquid crystal of achiral molecular dimers. *Proceedings of the National Academy of Sciences of the United States of America*. 2013;110:15931-6.
38. Borshch V, Kim YK, Xiang J, Gao M, Jákli A, Panov VP, Vij JK, Imrie CT, Tamba MG, Mehl GH, Lavrentovich OD. Nematic twist-bend phase with nanoscale modulation of molecular orientation. *Nature Communications*. 2013;4:2635.

39. Chen D, Nakata M, Shao RF, Tuchband MR, Shuai M, Baumeister U, Weissflog W, Walba DM, Glaser MA, MacLennan JE, Clark NA. Twist-bend heliconical chiral nematic liquid crystal phase of an achiral rigid bent-core mesogen. *Phys Rev E*. 2014;89:022506.
40. Xiang J, Shiyanovskii SV, Imrie CT, Lavrentovich OD. Electrooptic Response of Chiral Nematic Liquid Crystals with Oblique Helicoidal Director. *Phys Rev Lett*. 2014;112:217801.
41. Xiang J, Li YN, Li Q, Paterson DA, Storey JMD, Imrie CT, Lavrentovich OD. Electrically Tunable Selective Reflection of Light from Ultraviolet to Visible and Infrared by Heliconical Cholesterics. *Adv Mater*. 2015;27:3014-8.
42. Salili SM, Xiang J, Wang H, Li Q, Paterson DA, Storey JMD, Imrie CT, Lavrentovich OD, Sprunt SN, Gleeson JT, Jákli A. Magnetically tunable selective reflection of light by heliconical cholesterics. *Phys Rev E*. 2016;94:042705.
43. Meyer RB. Distortion of a Cholesteric Structure by a Magnetic Field. *Appl Phys Lett*. 1969;14:208-9.
44. Gennes PGd. Calcul de la distorsion d'une structure cholesterique par un champ magnetique. *Solid State Commun*. 1968;6:163-5.
45. Lydon J. Chromonic liquid crystalline phases. *Liq Cryst*. 2011;38:1663-81.
46. Zhou S, Nastishin YA, Omelchenko MM, Tortora L, Nazarenko VG, Boiko OP, Ostapenko T, Hu T, Almasan CC, Sprunt SN, Gleeson JT, Lavrentovich OD. Elasticity of Lyotropic Chromonic Liquid Crystals Probed by Director Reorientation in a Magnetic Field. *Phys Rev Lett*. 2012;109:037801.
47. Zhou S, Cervenka AJ, Lavrentovich OD. Ionic-content dependence of viscoelasticity of the lyotropic chromonic liquid crystal sunset yellow. *Phys Rev E*. 2014;90:042505.
48. Taratuta VG, Hurd AJ, Meyer RB. Light-Scattering Study of a Polymer Nematic Liquid-Crystal. *Phys Rev Lett*. 1985;55:246-9.
49. Dietrich CF, Collings PJ, Sottmann T, Rudquist P, Giesselmann F. Extremely small twist elastic constants in lyotropic nematic liquid crystals. *Proceedings of the National Academy of Sciences of the United States of America*. 2020;117:27238-44.
50. Meyer RB. Macroscopic phenomena in nematic polymers. In: Ciferri A, Krigbaum WR, Meyer RB, editors. *Polymer Liquid Crystals*. New York/London: Academic Press, Inc.; 1982. p. 133-85.
51. Koizumi R, Li BX, Lavrentovich OD. Effect of Crowding Agent Polyethylene Glycol on Lyotropic Chromonic Liquid Crystal Phases of Disodium Cromoglycate. *Crystals*. 2019;9:160.
52. Koizumi R, Golovaty D, Alqarni A, Li BX, Sternberg PJ, Lavrentovich OD. Topological transformations of a nematic drop. *Science Advances*. 2023;9:eadf3385.
53. Jockusch H, Dress A. From sphere to torus: A topological view of the metazoan body plan. *B Math Biol*. 2003;65:57-65.
54. Edelman DB, McMenamin M, Sheesley P, Pivar S. Origin of the vertebrate body plan via mechanically biased conservation of regular geometrical patterns in the structure of the blastula. *Prog Biophys Mol Bio*. 2016;121:212-44.
55. Lavrentovich OD. Topological defects in dispersed liquid crystals, or words and worlds around liquid crystal drops. *Liq Cryst*. 1998;24:117-25.
56. Ondris-Crawford R, Boyko EP, Wagner BG, Erdmann JH, Žumer S, Doane JW. Microscope Textures of Nematic Droplets in Polymer Dispersed Liquid-Crystals. *J Appl Phys*. 1991;69:6380-6.
57. Wei WS, Xia Y, Ettinger S, Yang S, Yodh AG. Molecular heterogeneity drives reconfigurable nematic liquid crystal drops. *Nature*. 2019;576:433-6.
58. Peddireddy K, Čopar S, Le KV, Mušević I, Bahr C, Jampani VSR. Self-shaping liquid crystal droplets by balancing bulk elasticity and interfacial tension. *Proceedings of the National Academy of Sciences of the United States of America*. 2021;118:e2011174118.
59. Lavrentovich OD, Nastishin YA. Division of Drops of a Liquid-Crystal in the Case of a Cholesteric-Smectic-a Phase-Transition. *Sov Phys JETP Letters*. 1984;40:1015-9.

60. Kleman M, Lavrentovich OD. *Soft Matter Physics: An Introduction*. New York: Springer; 2003.
61. Li ZL, Lavrentovich OD. Surface Anchoring and Growth-Pattern of the Field-Driven 1st-Order Transition in a Smectic-a Liquid-Crystal. *Phys Rev Lett*. 1994;73:280-3.
62. Mertelj A, Cmok L, Sebastián N, Mandle RJ, Parker RR, Whitwood AC, Goodby JW, Čopič M. Splay Nematic Phase. *Phys Rev X*. 2018;8:041025.
63. Chen X, Korblova E, Dong DP, Wei XY, Shao RF, Radzihovsky L, Glaser MA, MacLennan JE, Bedrov D, Walba DM, Clark NA. First-principles experimental demonstration of ferroelectricity in a thermotropic nematic liquid crystal: Polar domains and striking electro-optics. *Proceedings of the National Academy of Sciences of the United States of America*. 2020;117:14021-31.
64. Meyer RB. Ferroelectric Liquid-Crystals - Review. *Mol Cryst Liq Cryst*. 1977;40:33-48.
65. Okano K. Electrostatic Contribution to the Distortion Free-Energy Density of Ferroelectric Liquid-Crystals. *Jpn J Appl Phys* 2. 1986;25:L846-L7.
66. Lee JB, Pelcovits RA, Meyer RB. Role of electrostatics in the texture of islands in free-standing ferroelectric liquid crystal films. *Phys Rev E*. 2007;75: 051701.
67. Chen X, Martinez V, Korblova E, Freychet G, Zhernenkov M, Glaser MA, Wang C, Zhu C, Radzihovsky L, MacLennan JE, Walba DM, Clark NA. The smectic Z_A phase: Antiferroelectric smectic order as a prelude to the ferroelectric nematic. *Proceedings of the National Academy of Sciences of the United States of America*. 2023;120:e2217150120.
68. Nishikawa H, Shiroshita K, Higuchi H, Okumura Y, Haseba Y, Yamamoto S-I, Sago K, Kikuchi H. A Fluid Liquid-Crystal Material with Highly Polar Order. *Adv Mater*. 2017;29:1702354.
69. Chen X, Zhu ZC, Magrini MJ, Korblova E, Park CS, Glaser MA, MacLennan JE, Walba DM, Clark NA. Ideal mixing of paraelectric and ferroelectric nematic phases in liquid crystals of distinct molecular species. *Liq Cryst*. 2022;49:1531-44.
70. Zhuang Z, MacLennan JE, Clark NA. Device Applications of Ferroelectric Liquid-Crystals - Importance of Polarization Charge Interactions. *P Soc Photo-Opt Ins*. 1989;1080:110-4.
71. Link DR, Chattham N, MacLennan JE, Clark NA. Effect of high spontaneous polarization on defect structures and orientational dynamics of tilted chiral smectic freely suspended films. *Phys Rev E*. 2005;71:021704.
72. Pattanaporkratana A. Textures and interactions between vortices in the 2D XY field of freely suspended SmC and SmC* liquid crystal films. Boulder, CO: University of Colorado; 2008.
73. Silvestre NM, Patrício P, da Gama MMT, Pattanaporkratana A, Park CS, MacLennan JE, Clark NA. Modeling dipolar and quadrupolar defect structures generated by chiral islands in freely suspended liquid crystal films. *Phys Rev E*. 2009;80:041708.
74. Dolganov PV, Dolganov VK, Cluzeau P. The effect of spontaneous polarization on two-dimensional elasticity of smectic liquid crystals. *J Exp Theor Phys+*. 2013;116:1043-9.
75. Chen X, Martinez V, Nacke P, Korblova E, Manabe A, Klasen-Memmer M, Freychet G, Zhernenkov M, Glaser MA, Radzihovsky L, MacLennan JE, Walba DM, Bremer M, Giesselmann F, Clark NA. Observation of a uniaxial ferroelectric smectic A phase. *Proceedings of the National Academy of Sciences of the United States of America*. 2022;119:e2210062119.
76. Basnet B, Rajabi M, Wang H, Kumari P, Thapa K, Paul S, Lavrentovich MO, Lavrentovich OD. Soliton walls paired by polar surface interactions in a ferroelectric nematic liquid crystal. *Nature Communications*. 2022;13:3932.
77. Kumari P, Basnet B, Wang H, Lavrentovich OD. Ferroelectric nematic liquids with conics. *Nature Communications*. 2023;14:748.
78. Thurston RN, Cheng J, Meyer RB, Boyd GD. Physical-Mechanisms of DC Switching in a Liquid-Crystal Bistable Boundary-Layer Display. *J Appl Phys*. 1984;56:263-72.
79. Nazarenko VG, Lavrentovich OD. Anchoring Transition in a Nematic Liquid-Crystal Composed of Centrosymmetric Molecules. *Phys Rev E*. 1994;49:R990-R3.

80. Ramdane OO, Auroy P, Forget S, Raspaud E, Martinot-Lagarde P, Dozov I. Memory-free conic anchoring of liquid crystals on a solid substrate. *Phys Rev Lett*. 2000;84:3871-4.
81. Lavrentovich OD, Rozhkov SS. Strings with Boojums at Their Ends - Topological Defects of a New Type in Nematic Liquid-Crystals. *Jetp Lett*+. 1988;47:254-8.
82. Apollonius of Perga, Heath TL. *Treatise on Conic Sections*: Cambridge University Press; 1896.
83. Jennings GA. *Modern geometry with applications*. New York: Springer-Verlag New York, Inc.; 1994.
84. Lavrentovich OD. Ferroelectric nematic liquid crystal, a century in waiting. *Proceedings of the National Academy of Sciences of the United States of America*. 2020;117:14629-31.
85. Kats EI. Combined Defects in Ferroelectric Nematics. *J Exp Theor Phys*+. 2021;132:641-8.
86. Hindmarsh MB, Kibble TWB. Cosmic Strings. *Rep Prog Phys*. 1995;58:477-562.
87. Makinen JT, Dmitriev VV, Nissinen J, Rysti J, Volovik GE, Yudin AN, Zhang K, Eltsov VB. Half-quantum vortices and walls bounded by strings in the polar-distorted phases of topological superfluid He-3. *Nature Communications*. 2019;10:237.
88. Volovik GE, Zhang K. String monopoles, vortex skyrmions, and nexus objects in the polar distorted B phase of ^3He . *Physical Review Research*. 2020;2:023263.
89. Friedel G, Grandjean F. Les liquides à conique focales. *Comptes rendus de l'Académie des Sciences*. 1910;151:762-5.
90. Friedel G, Grandjean F. Structure des liquides à coniques focales. *Comptes rendus de l'Académie des Sciences*. 1911;152-155:322.
91. Friedel G. Les états mésomorphes de la matière *Ann Phys (Paris)*. 1922;19:273-474.
92. Rosenblatt CS, Pindak R, Clark NA, Meyer RB. Parabolic Focal Conic - New Smectic a Defect. *J Phys-Paris*. 1977;38:1105-15.
93. Kléman M. Energetics of Focal Conics of Smectic Phases. *J Phys-Paris*. 1977;38:1511-8.
94. Luk'yanchuk I, Tikhonov Y, Razumnaya A, Vinokur VM. Hopfions emerge in ferroelectrics. *Nature Communications*. 2020;11:2433.
95. Ackerman PJ, Smalyukh II. Static three-dimensional topological solitons in fluid chiral ferromagnets and colloids. *Nat Mater*. 2017;16:426-32.
96. Smalyukh II. Review: knots and other new topological effects in liquid crystals and colloids. *Rep Prog Phys*. 2020;83:106601.
97. Wu JS, Smalyukh II. Hopfions, heliknotons, skyrmions, torons and both abelian and nonabelian vortices in chiral liquid crystals. *Liquid Crystals Reviews*. 2022;10.1080/21680396.2022.2040058.
98. Cladis PE, Kléman M. Non-Singular Disclinations of Strength $S = +1$ in Nematics. *J Phys-Paris*. 1972;33:591-8.
99. Meyer RB. Existence of Even Indexed Disclinations in Nematic Liquid-Crystals. *Philos Mag*. 1973;27:405-24.
100. Karcz J, Herman J, Rychłowiec N, Kula P, Górecka E, Szydłowska J, Majewski PW, Pocięcha D. Spontaneous polar and chiral symmetry breaking in ordered fluids - heliconical ferroelectric nematic phases. *arXiv*. 2023:2311.18552.
101. Lavrentovich OD. Electromagnetically tunable cholesterics with oblique helicoidal structure. *Opt Mater Express*. 2020;10:2415-24.